Optical scattering, absorption, and polarization of healthy and neovascularized human retinal tissues

Dhiraj K. Sardar
Ray M. Yow
University of Texas at San Antonio
Department of Physics and Astronomy
San Antonio, Texas 78249-0697

Andrew T. C. Tsin
Ratna Sardar
University of Texas at San Antonio
Department of Biology
San Antonio, Texas 78249

Abstract. The optical scattering, absorption, and polarization properties of human retinal tissues are investigated for a number of laser wavelengths in the visible range. The indices of refraction of these tissues are determined by applying Brewster's law. The inverse adding doubling method based on the diffusion approximation and radiative transport theory is applied to the measured values of total diffuse transmission, total diffuse reflection, and index of refraction to determine the optical absorption, scattering, and scattering anisotropy coefficients of the intact retinal tissues from healthy and diseased (neovascularized) human eyes. The polarization studies show that the retinal tissues possess significant intrinsic polarization characteristics, that are more pronounced in diseased tissues than in healthy tissues.
 [DOI: 10.1117/1.2065867]

Keywords: lasers; human retinal tissues; optical properties; neovascularization; polarization.

Paper SS04224R received Nov. 22, 2004; revised manuscript received May 6, 2005; accepted for publication May 6, 2005; published online Oct. 4, 2005.

1 Introduction

There have been some past studies on ocular melanin.[1,2] Studies of optical absorption and scattering on ocular fundus tissues were also reported by Hammer et al.[3] However, to the best of our knowledge, a systematic investigation of the optical scattering, optical absorption, and polarization properties of intact human retinal tissues has not been done. In this paper, we present an in-depth characterization of the optical absorption, scattering, and polarization properties of healthy and diseased human retinal tissues.

Since medical laser applications for ocular diseases have steadily increased over the past several years, understanding the fundamental optical properties of ocular tissues has become imperative because they influence the distribution and propagation of light in laser-irradiated tissues. Due to the complex nature of retinal tissues, both the absorption and scattering properties of these tissues must be understood thoroughly for medical applications of lasers. The quantitative distribution of light intensity in biological media can be obtained from the solution of the radiative transport equation.[4] The details of the radiative transport equation and the application of the Henyey-Greenstein scattering approximation to biological media can be found in Ref. 5. Although there is no analytical solution to the transport equation for biological media due to the inherent inhomogeneities and irregularities in their physical shapes, only an approximate solution can be obtained by assuming homogeneity and regular geometry of the medium, and thereby an estimate of light intensity distribution can be obtained by solving the radiative transport equation. The values of absorption, scattering, and scattering anisotropy coefficients are required for even the approximate solution to the transport equation. Therefore, appropriate experimental methods are necessary to measure these optical properties. Although a single measurement of the transmission through a sample of known thickness provides only the total attenuation coefficient for Beer's law of exponential decay, it is impossible to separate the loss due to absorption from the loss due to scattering. This problem has been resolved, to some extent, by the 1-D, two-flux Kubelka-Munk model,[6] which has been widely used to determine the absorption and scattering coefficients of biological media,[7–12] provided the scattering is significantly dominant over the absorption. This model provides simple mathematical expressions for determining the optical parameters from the diffuse reflection and diffuse transmission measurements. In the past, researchers have applied the diffusion approximation to the transport equation to study biological media.[13–15] Also, based on the Kubelka-Munk model and diffusion approximation, an excellent experimental method has been developed by van Gemert et al. (see Ref. 16 and the references therein) and van Gemert and Star[17] for determining the absorption and scattering coefficients and the scattering anisotropy factor.

More recently, an important numerical approach known as the inverse adding doubling (IAD) method[5] was introduced to solve the transport equation.[4] The IAD method provides more accurate estimates of optical properties for turbid media than any other models previously used. Thus, in this study, the IAD method is employed to determine both the absorption and scattering coefficients. A short synopsis of the IAD model is provided here. Two dimensionless quantities albedo (a) and optical depth (τ) are obtained from the IAD method; these quantities are defined as follows:

Address all correspondence to Dhiraj K. Sardar, University of Texas at San Antonio, Department of Physics and Astronomy, 6900 North Loop 1604 West, San Antonio, TX 78249-0697. Tel.: (210) 458-5748; Fax: (210) 458-5748; E-mail: dsardar@utsa.edu

1083-3668/2005/10(5)/051501/8/$22.00 © 2005 SPIE

$$a = \frac{\mu_s}{\mu_a + \mu_s}, \tag{1}$$

and

$$\tau = t(\mu_a + \mu_s), \tag{2}$$

where μ_a is the absorption coefficient, μ_s is the scattering coefficient, and t is the physical thickness of the sample. The measured values of total diffuse reflectance and total diffuse transmittance are applied to the IAD algorithm to determine the optical absorption and scattering coefficients of human retinal tissues.

Recently, there has been a considerable interest in the investigation of polarized light in highly scattering biological media. For example, Schmitt et al.[18] suggested the use of transmitted polarized light for imaging tissue heterogeneities. Anderson,[19] Jacques et al.,[20] and Demos and Alfano[21] investigated the use of backscattered light for surface and beneath-the-surface imaging. Recently, Jacques et al. showed that the polarized light can be used effectively to image skin in which the structural details of the superficial layers can be easily identified.[22] Hielscher et al.[23,24] demonstrated that backscattered linearly polarized light could be used to determine the fundamental optical properties such as scattering coefficient, scattering anisotropy factor, and average particle size of polystyrene spheres and biological cell suspensions. Hielscher et al. also demonstrated that cancerous rat fibroblast cells can be distinguished from noncancerous cells by measuring backscattered circularly polarized light and using the Mueller-matrix method.[25] An excellent study by Ducros et al. indicates that polarization-sensitive optical coherence tomography can determine the retinal nerve fiber layer thickness and birefringence; the retinal polarization can therefore be employed to evaluate the effect of glaucomatous damage to the nerve fiber layer in retina.[26]

The optical properties of biological tissues are related to their constituents. During neovascularization, the proliferation of retinal vessels and the increased blood in capillaries could change the optical properties of tissue. Therefore, for medical laser applications, an in-depth knowledge of tissue optical properties is imperative not only for therapeutic and clinical purposes, but also for noninvasive diagnostic purposes. The optical polarimetry study of ocular tissues is especially significant for noninvasive diagnosis of neovascularized ocular tissues. Blindness in diabetic retinopathy results when the macula is involved, but it also follows vitreous hemorrhages, retinal detachment, and glaucoma.[27] The neovascularization of retina, a predominant feature of diabetic retinopathy, is associated with the proliferation and migration of astrocytes that grow around the new vessels to form delicate white veils. The proliferating fibrovascular and glial tissues often cause retinal detachment and blindness. Hypertensive and arteriolar retinopathy are generally associated with diabetic retinopathy.[28]

Currently, tissue polarimetry has become an exciting area of research in tissue optics and is expected to generate a great deal of interest in biomedical applications. Laser light is intrinsically polarized, and many biological tissues or molecules such as collagen, muscle fibers, keratin, retina, melanin, and glucose are known to be birefringent, and thereby possess polarization properties. In addition, biological scatterers such as cell nuclei and mitochondria alter light polarization on each scattering event according to the geometry and optical properties of the scatterers. Polarization can therefore provide a novel mode of early detection and diagnosis of ocular diseases such as diabetic retinopathy and macular degeneration. Recent studies have shown that important information on biological media can be obtained by shining a polarized laser light through the sample and then analyzing the state of polarization of the diffusely backscattered light.[29] Several researchers have also demonstrated that scanning laser polarimetry can be a useful tool for the assessment of the retinal nerve fiber layer, which plays an important role in the early detection of glaucoma.[30–32] To develop an optical technique for tissue diagnosis and therapeutic applications, it is necessary to understand the relationship between the optical and biological properties of tissue.

2 Materials and Methods

2.1 *Tissue Sample Preparation*

One pair of healthy human eyes and one pair of diseased (neovascularized) human eyes were obtained from the National Disease Research Interchange (NDRI). The samples were procured under the stipulation that both sets of eyes were from donors with similar ages and were shipped on ice to preserve their physiological properties. On arrival of the healthy and diseased human eyes, these eyes were carefully dissected using forceps and a scalpel to prepare retinal tissue samples for optical measurements. The cornea, lens, and vitreous humor was removed from each eye sample. For each sample, the retina was then separated from the choroid and placed between a pair of glass slides separated by three layers of cover slips (spacers) on each side. Each spacer was measured to be about 0.09 ± 0.01 mm. Special care was taken to fill in the space with the retinal tissues between the spacers. The purpose of placing the spacers was to prevent the glass slides from squeezing the tissue from its original, native shape to a compressed form. The thicknesses of the samples were measured using a digital micrometer. After placing the retinal tissue sample in between two glass slides, the total thickness of the system was measured. The thickness of the retinal sample was obtained by subtracting the thickness of the slides only from the thickness of the combined system. The thicknesses of both healthy and diseased retinal layers were found to be approximately 0.27 mm each. Note, however, that any difference between the thicknesses of diseased and healthy retinal layers was so small that it could not be determined with precision due to the limitation of the measuring device and also due to the uncertainty in measurements. Therefore, the value of 0.27 mm for the thicknesses of diseased and healthy retinal layers is used in all calculations.

The intact retina from each human eye was used for optical measurements. Although it was our intent to separate the retina from the choroid, it was difficult to obtain only retina while lifting the intact retina from the eye cup. It is expected to have a part of choroid left on the retinal sample during its preparation. Therefore it is assumed that retinal samples used in our measurements consisted of the following layers: (1) nerve fiber, (2) retinal blood vessels, (3) photoreceptor layer, (4) retinal pigment epithelium, and (5) choroid.

A small amount of vacuum grease was applied in between the glass slides to seal the open space between them so that the retinal tissue was kept moist and retained its space between the glass slides. These precautions were necessary to maintain the integrity of tissue's physiological properties and also to make sure that its optical properties did not change due to the inadvertant compression and/or dehydration of the sample. Special attention was also paid in mounting the samples for optical measurements so that the laser light was directed into the retinal tissue samples from inside the eye cup.

2.2 *Index of Refraction Measurement*

The indices of refraction of the retinal tissues were determined using Brewster's law. According to Brewster's law, the index of refraction (n) of the tissue can be determined by the following expression:

$$\tan \theta_p = n, \tag{3}$$

where θ_p is the polarizing angle or Brewster's angle of incidence. The experimental details can be found in Ref. 33.

2.3 *Measurement of Scattering Anisotropy*

Using an independent experimental technique, the scattering anisotropy coefficient (g) can also be obtained from the measurements of scattered light intensities (I) at various scattering angles (θ) using a goniometer table, assuming single scattering of the photons. The scattering anisotropy coefficient g is given by the average cosine of the scattering angle (θ) according to

$$g = \frac{\sum_i (\cos \theta_i) I_i}{\sum_i I_i}, \tag{4}$$

where the sums are taken over all values (i) of the scattering angles and intensities. The scattering anisotropy coefficient (g) was obtained by irradiating the individual ocular tissue sample with a HeNe laser (Uniphase model 1101P) with a power of 3.0 mW, beam diameter of 2.5 mm, and beam divergence of 1.3 mrad. The sample was placed in the sample holder affixed to the center of the goniometer table. The measurements were taken using an Oriel (model 77341) photomultiplier tube (PMT) mounted at the edge of the goniometer table. The PMT was powered by a Bertan (model 215) power supply. The HeNe laser beam was aligned at a right angle with respect to the plane of the tissue sample, and the PMT was attached to an adjustable pointer, which could be rotated around the circular goniometer table to measure the scattered intensities at different angles. Further experimental details can be found in Ref. 33.

2.4 *Measurement of Diffuse Reflectance and Transmittance*

The total diffuse reflectance and total diffuse transmittance were measured using two identical integrating spheres (Oriel model 70451). The tissue sample was placed in a specially designed holder that coupled the two integrating spheres. The measurements were performed on the retinal tissues at 514, 501, 488, and 476 nm from an argon ion laser (Spectra Physics model 2025). Although the maximum output power of the argon ion laser varied from 1 to 2 W, the average output power was kept at its minimum value of about 5 mW for all optical measurements. The laser beam diameter at $1/e^2$ was 1.25 mm and beam divergence was 0.70 mrad at 488 nm.

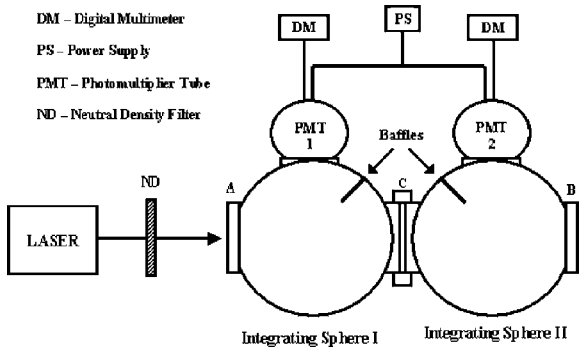

Fig. 1 Experimental schematic for the total diffuse reflection and total diffuse transmission measurements on the human retinal tissues.

A schematic of the experimental setup for measuring the total diffuse reflectance and total diffuse transmittance is shown in Fig. 1. The experimental setup was similar to that used by Beek et al.[34] The laser beam was directed into entrance port A of integrating sphere 1, whose exit port is coupled with the entrance port of integrating sphere 2; the sample was mounted at coupling port C situated in between the two integrating spheres. Exit port B of integrating sphere 2 was covered with a cap with a reflective surface identical to that of the integrating spheres. The diameter of each sphere was 6 in. and each port had a diameter of 1 in. Light leaving the sample reflected multiple times from the inner surfaces of the spheres before reaching the PMTs. The baffles within the spheres shielded the PMTs from receiving the direct reflected and transmitted light from the sample. Port A was equipped with a variable aperture so that the beam diameter could be appropriately controlled. The reflected and transmitted light intensities were detected by two identical PMTs (Oriel model 77341); these were attached to the two measuring ports of the integrating spheres I and II. The PMTs were powered by a common power supply (Bertan model 215). The signals from the PMTs were measured by two identical Fluke digital multimeters (model 77 series II). The measured light intensities were then utilized to determine the total diffuse reflectance R_d and total diffuse transmittance T_d by the following expressions:

$$R_d = \frac{X_r - Y}{Z_r - Y}, \tag{5}$$

and

$$T_d = \frac{X_t - Y}{Z_t - Y}, \tag{6}$$

where X_r is the reflected light intensity detected by PMT 1 with sample at C; Z_r is the incident intensity detected by PMT 1 without the sample at C, while the reflective surface is placed at the exit port of integrating sphere I; X_t is the transmitted light intensity detected by PMT 2 with the sample at C;

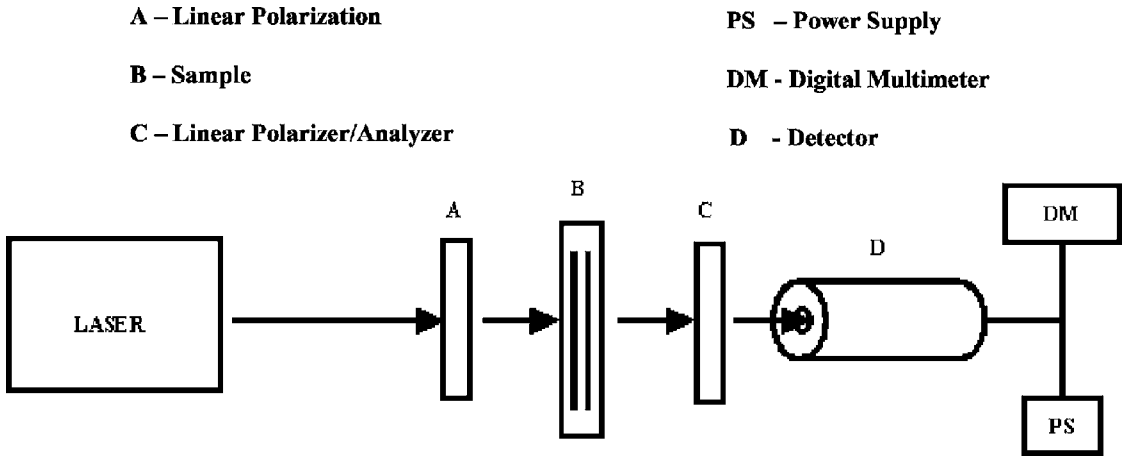

Fig. 2 Experimental schematic for polarization measurements on human retinal tissues.

Z_t is the incident light intensity detected by PMT 2 with no sample at C and with a reflective surface at B; and Y is the correction factor for the stray light measured by PMTs 1 and 2 with no sample at C nor the reflective surface at B.

2.5 *IAD Method*

To solve the radiative transport equation, the IAD algorithm[5] must be supplied with the experimentally determined values of the total diffuse reflectance (R_d) and total diffuse transmittance (T_d), along with the values of the index of refraction, the anisotropy coefficient, and the physical thickness of the sample. The IAD program determines the optical properties of the sample using the values of R_d and T_d. A set of optical properties is guessed by the IAD program and the values of R_d and T_d are calculated iteratively until these values match with the measured values of R_d and T_d. When the IAD program finds the match between the calculated and the measured values of R_d and T_d, the optical properties of the sample are found; these values are then given as output of the program in terms of the two dimensionless quantities: a and τ, defined in Eqs. (1) and (2), respectively. The values of a and τ provided by the IAD method are then used to calculate the absorption coefficient (μ_a) and scattering coefficient (μ_s) using Eqs. (1) and (2).

2.6 *Monte Carlo Simulation*

Accuracy of the measurements of the total diffuse reflectance (R_d) and total diffuse transmittance (T_d) used in the IAD method to determine the optical absorption coefficient (μ_a) and scattering coefficient (μ_s) are verified by the Monte Carlo (MC) simulation technique, which uses a stochastic model to simulate light interaction in biological media. The values of μ_a and μ_s determined by the IAD method, along with the values of n and g, are input into the MC simulation model, which in turn determines R_d and T_d. These values are then compared with those measured using the integrating spheres. A detailed description of the MC model can be found in Ref. 35.

2.7 *Polarization Measurements*

The experimental setup for the polarization measurements in human retinal tissues is shown in Fig. 2. The experimental setup was similar to that employed by Sardar et al.[33] A He–Ne laser (Uniphase model 1101P) beam with a power of 3.0 mW, a beam diameter of 2.5, and a beam divergence of 1.3 mrad mm was passed through a linear polarizer placed in front of the sample beyond which was placed a second linear polarizer (analyzer). The polarizers were obtained from the Oriel Corporation (Oriel model 25010). Behind the analyzer was placed a photodiode detector that was provided a low bias voltage from a power supply (Cenco model 31382); the photodiode was connected to a multimeter (Fluke model 77 series II). The polarizer (without the sample and analyzer in the light path) was rotated until the maximum laser light intensity was obtained, making sure that the laser beam is completely polarized. Once the maximum laser intensity was achieved, the analyzer was placed behind a pair of blank slides (without the sample between them). The analyzer was then rotated to maximize the light intensity so that the transmission axes of the polarizer and analyzer were parallel. Therefore, the reference condition was established with a pair of blank glass slides placed at the sample position. The blank slides were then replaced by the retinal tissue sample placed in between the polarizer and analyzer. Due to the birefringence property of retinal tissue, the polarization plane shifts; the polarization shift was then measured by rotating the analyzer until the maximum intensity was obtained. The measurements of polarization shifts and intensities of the scattered polarized light were taken at three different locations on each sample; the average of the three measurements was taken.

3 Results and Discussion

The indices of refraction (n) of retinal tissues from the healthy and diseased human eyes were measured by the Brewster's method at 450, 500, 550, and 600 nm from a xenon lamp. The measured n values varied from 1.34 to 1.38. Measurements were repeated three times at each laser wavelength, and the values agreed to within about 5%. For all of the IAD calculations, we used the average value of 1.36 for

Table 1 Wavelength-dependent absorption coefficient (μ_a), scattering coefficient (μ_s), total attenuation coefficient (μ_t), mean-free-path ($1/\mu_t$), albedo (a), and optical depth (τ) as determined by IAD using the measured diffuse reflectance (R_d) and diffuse transmittance (T_d) for human retina. The margin of error is given to the right of each measured value.

		Experimental		IAD					
Condition	Wavelength (nm)	R_d	T_d	a	τ	$\mu_a\,(\mathrm{cm}^{-1})$	$\mu_s\,(\mathrm{cm}^{-1})$	$\mu_t\,(\mathrm{cm}^{-1})$	$1/\mu_t\,(\mathrm{cm})$
Healthy	476	0.140± 0.003	0.74± 0.01	0.977	1.591	1.37	57.56	58.92	0.017
	488	0.130± 0.006	0.72± 0.02	0.969	1.582	1.81	56.8	58.61	0.0171
	501	0.099± 0.002	0.71± 0.05	0.937	1.555	3.61	53.99	57.6	0.0174
	514	0.091± 0.002	0.74± 0.04	0.926	1.549	4.23	53.12	57.35	0.0174
Diseased	476	0.330± 0.005	0.35± 0.06	0.99	9.484	3.45	347.81	351.26	0.0028
	488	0.176± 0.004	0.33± 0.06	0.964	5.856	7.83	209.05	216.88	0.0046
	501	0.153± 0.004	0.35± 0.05	0.955	4.965	8.19	175.7	183.89	0.0054
	514	0.142± 0.004	0.41± 0.05	0.951	3.813	6.89	134.33	141.22	0.0071

all retinal tissues. The average scattering anisotropy coefficient of retinal tissues was determined from the goniometric measurements on the healthy sample and was found to be approximately 0.79, indicating the presence of profound forward-scattering in the retinal tissues. The diseased tissue was assumed to be of the same makeup as the healthy tissue, only with more scatterers. Hence the anisotropy for the diseased tissue was assumed to be 0.79 as well.

The total diffuse reflectance (R_d) and total diffuse transmittance (T_d) were measured on the retinal tissue at 476, 488, 501 and 514 nm from the argon ion laser. These values of R_d and T_d are given in Table 1. The margin of errors of the measurements of R_d and T_d are also given in Table 1. These values, along with the measured value of the index of refraction and the scattering anisotropy coefficient, were input into the IAD program. The output of the IAD program were the dimensionless quantities a and τ, defined by Eqs. (1) and (2), respectively. The absorption and scattering coefficients were then calculated from the values of a and τ and the thickness t of the sample. The absorption coefficient (μ_a), scattering coefficient (μ_s), total attenuation coefficient ($\mu_t = \mu_a + \mu_s$), penetration depth ($1/\mu_t$), albedo (a), and optical depth (τ) for the retinal tissues are given in Table 1. Note, however, that the healthy sample was measured to be approximately 0.27 mm; while the IAD method provided us with a value of $1/\mu_s$ of approximately 0.20 mm. This shows that our assumption of nearly single scattering phenomenon in our experimental measurements for g is valid only within the experimental uncertainties. The total attenuation coefficients of the healthy and diseased tissues are plotted as a function of laser wavelength in Fig. 3, which shows that the total attenuation coefficients for diseased retinal tissues are significantly wavelength dependent, whereas the total attenuation coefficients for the healthy retinal tissues are less wavelength dependent. Note, however, that the range of wavelengths covered in this paper is too narrow to observe the wavelength dependencies of the healthy tissues. The experimental values of total diffuse reflectance (R_d) and total diffuse transmittance (T_d) used to obtain absorption coefficient (μ_a) and scattering coefficient (μ_s) from the IAD were compared with those generated by the MC simulation technique. These values are given in Table 2 for both the healthy and diseased retinal tissues. The percentage differences between the values obtained from the experiment and the MC method are also given in Table 2. These

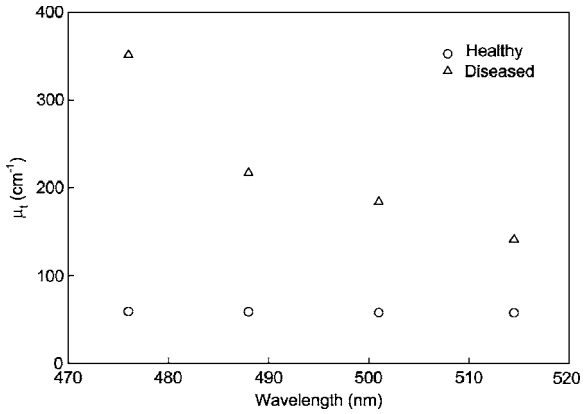

Fig. 3 Total attenuation coefficient as a function of wavelength for healthy and diseased retinal tissues.

Table 2 The diffuse reflectance (R_d) and diffuse transmittance (T_d) of human retina as determined by the experimental and MC techniques.

Condition	Wavelength (nm)	Experimental		MC		Percent Difference	
		R_d	T_d	R_d	T_d	R_d	T_d
Healthy	476	0.14	0.74	0.098	0.85	35.5	13.6
	488	0.13	0.72	0.094	0.84	32.5	15.1
	501	0.099	0.71	0.079	0.79	22.1	11.2
	514	0.091	0.74	0.075	0.78	19.1	9.5
Diseased	476	0.33	0.35	0.417	0.4	23.3	14.3
	488	0.176	0.33	0.237	0.45	29.4	29.7
	501	0.153	0.35	0.2	0.48	26.9	31.6
	514	0.142	0.41	0.167	0.57	16.3	32.5

values range from approximately 10 to 30%; these can be considered reasonable due to experimental uncertainties, and also considering the complexity of the healthy and diseased retinal tissues. In both the healthy and diseased retinal tissues, the scattering coefficients are found to be significantly higher than the absorption coefficients; the higher values of scattering coefficients can be attributed to some inadvertant cross-contamination of the retina with melanin granules from the retinal pigment epithelium (RPE) during sample preparation. Note also that the diseased eyes have both higher absorption and higher scattering. The increased number of localized neovascularizations in the diseased retinal tissues could be the source for stronger scattering. Note, however, that even though it does not account for the light that could be lost at the edges of the sample, the IAD method has a number of advantages, such as it works for any combination of optical properties, it takes into account all the interactions of a sample sandwiched between glass slides, it incorporates the effects of the integrating spheres on the measured values, and it has a reasonable trade-off between accuracy and speed. Further details can be found in Ref. 5.

The measured polarization shifts ($\Delta\theta$) and intensities (I) of the scattered polarized light in healthy and neovascularized (diseased) human retinal tissues are given in Table 3. The average polarization shifts and average intensities for the healthy and neovascularized human retina are shown in Figs. 4 and 5. The results presented in Figs. 4 and 5 clearly suggest that the polarization shifts are more pronounced for the diseased retina than those for the healthy retina, while the intensities of the scattered light in diseased retinal tissue were smaller than in the healthy tissues. The higher polarization shifts in the diseased retinal tissues can be attributed to the structural changes due to neovascularization. The decrease in intensities of the scattered polarized light in the diseased (neovascularized) tissues is likely due to the enhanced scattering. This observation is supported by the results given in Table 1, which shows that the scattering coefficient of the diseased retinal tissue is much higher than that of the healthy tissue for each laser wavelength. The observed variations in polarization shifts between the left and right eyes could be attributed to the physiological differences in the eyes. Also, the small differences in the measurements at different locations can be due to the minuscule differences in thicknesses of the tissue samples.

In conclusion, the actual values of the absorption and scattering coefficients for the retinal tissues reported in this paper could have significant importance for practical applications requiring the prediction of light transport through pigmented tissue where the degree of pigmentation at the target sites may vary. Variable pigmentation obviously complicates the laser dosimetry for such treatment modes, because the amount of light delivered will have to be adjusted based on the amount of tissue pigmentation to achieve some standard clinical effect.[2] The tissue polarization study also is of particular im-

Table 3 Comparison of the average polarization shift ($\Delta\theta$) and average intensity (I) between the healthy and diseased retinal tissues for the human left and right eyes at 632.8 nm.

Condition	Eye	$\Delta\theta$ (deg)	Avg. $\Delta\theta$ (deg)	I (mV)	Avg. I (mV)
Healthy	Left	2.8±0.4	2.6	307±6	310
	Right	2.4±0.4		313±3	
Diseased	Left	5.8±0.5	5.8	274±5	275
	Right	5.8±0.4		275±5	

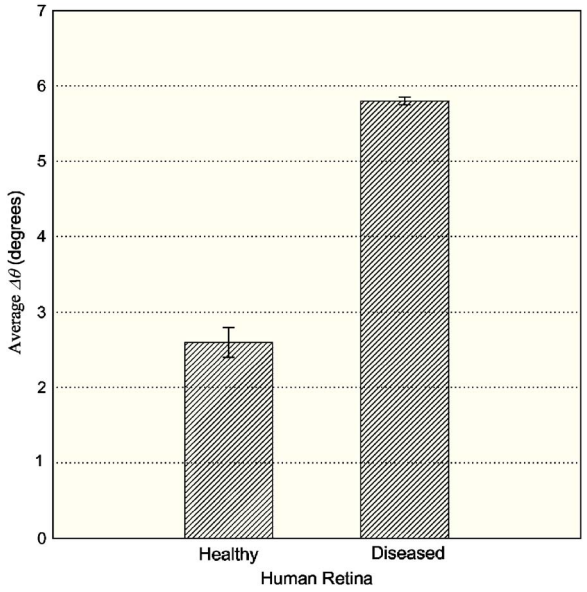

Fig. 4 Average polarization shift versus physiological condition of human retinal tissues; experimental error is shown in the bar graph.

portance because it offers a model for noninvasive diagnosis of neovascularized retinal as well as systemic diseases. Therefore, further investigation of different types ocular tissues, especially from human eyes at different pathological stages, is imperative for better understanding as well as the development of quantitative and noninvasive techniques for diagnosis of ocular diseases. Finally, note that the diseased retinal tissues possess the strong polarization characteristics.

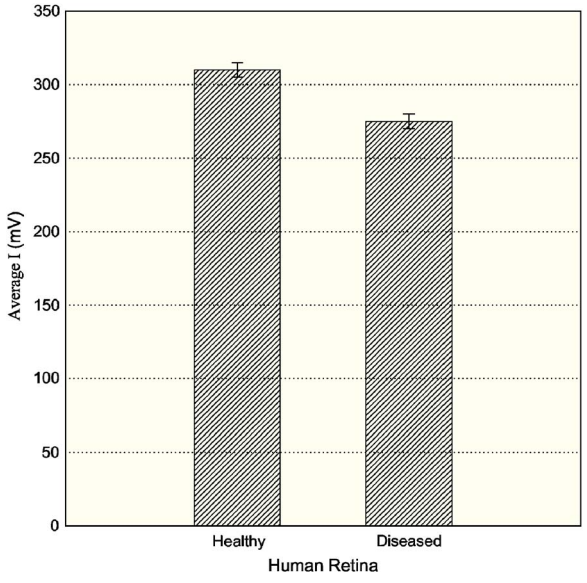

Fig. 5 Average intensity of scattered (polarized) light versus physiological condition of human retinal tissues; experimental error is shown in the bar graph.

Acknowledgments

This work was supported by the National Science Foundation (NSF)-sponsored Center for Biophotonics Science and Technology (CBST) at the University of California at Davis. One of the authors (DKS) would like to gratefully acknowledge the support by the University of Texas at San Antonio (UTSA) Faculty Development Award. The authors would like to thank Elia Villazana for preparing the tissue samples used in this study and also acknowledge Felipe Salinas for taking the data. The authors would also like to thank Scott Prahl (Oregon Medical Laser Center) for the use of the inverse adding doubling (IAD) source code and Steven L. Jacques (Oregon Medical Laser Center) and Lihong Wang (Texas A&M University) for the use of the source code for the Monte Carlo model. The source codes for both of these programs are available at http: //omlc.ogi.edu/software/.

References

1. T. Sarna, "Properties and function of the ocular melanin—a photobiophysical view," *J. Photochem. Photobiol., B* **12**, 215–258 (1992).
2. D. K. Sardar, M. L. Mayo, and R. D. Glickman, "Optical characterization of melanin," *J. Biomed. Opt.* **6**, 404–411 (2001).
3. M. Hammer, A. Roggan, D. Schweitzer, and G. Muller, "Optical properties of ocular fundus tissues—an in vitro study using the double-integrating-sphere technique and inverse Monte Carlo simulation," *Phys. Med. Biol.* **40**, 963–978 (1995).
4. S. Chandrasekhar, *Radiative Transfer*, Dover, New York (1960).
5. S. A. Prahl, M. J. C. Van Gemert, and A. J. Welch, "Determining the optical properties of turbid media by using the inverse adding-doubling method," *Appl. Opt.* **32**, 559–568 (1993).
6. P. Kubelka, "New contributions to the optics of intensely light-scattering materials, Part I," *J. Opt. Soc. Am.* **38**, 448–457 (1948).
7. F. Kottler, "Turbid media with plane-parallel surfaces," *J. Opt. Soc. Am.* **50**, 483–490 (1960).
8. S. Wan, R. R. Anderson, and J. A. Parish, "Analytical modeling for the optical properties of the skin with in vitro and in vivo applications," *Photochem. Photobiol.* **34**, 493–499 (1981).
9. R. R. Anderson and J. J. Parish, "The optics of human skin," *J. Invest. Dermatol.* **77**, 13–19 (1981).
10. S. Ertefai and A. E. Profio, "Spectral transmittance and contrast in breast diaphanography," *Med. Phys.* **12**, 393–400 (1985).
11. M. J. C. van Gemert, R. Verdaasdonk, E. G. Stassen, G. A. C. M. Schets, G. H. M. Gijsbers, and J. J. Bonnier, "Optical properties of human blood vessel wall and plaque," *Lasers Surg. Med.* **5**, 235–237 (1985).
12. M. R. Prince, F. T. Deutsch, R. Margolis, M. M. Mathews-Roth, J. A. Parrish, and A. S. Oseroff, "Preferential light absorption in atheromas: Implication for laser angioplasty," *J. Clin. Invest.* **78**, 295–302 (1978).
13. A. Ishimaru, *Wave Propagation and Scattering in Random Media*, Vol. 1, Academic Press, New York (1978).
14. L. Reynolds, C. C. Johnson, and A. Ishimaru, "Diffuse reflectance from a finite blood medium: application to the modeling of fiberoptic catheters," *Appl. Opt.* **15**, 2059–2067 (1978).
15. R. A. J. Groenhuis, H. A. Ferwerda, and J. J. Ten Bosch, "Scattering and absorption of turbid materials determined from reflection measurements. 1: Theory," *Appl. Opt.* **22**, 2456–2462 (1983).
16. M. J. C. van Gemert, A. J. Welch, W. M. Star, and M. Motamedi, "Tissue optics for a slab geometry in diffusion approximation," *Lasers Med. Sci.* **2**, 295–302 (1987).
17. M. J. C. van Gemert and W. M. Star, "Relations between the Kubelka-Munk and transport equation models for anisotropic scattering," *Lasers Life Sci.* **1**, 287–298 (1987).
18. J. M. Schmitt, A. H. Gandjbakhche, and R. F. Bonner, "Use of polarized-light to discriminate short-path photons in a multiply scattering medium," *Appl. Opt.* **31**, 6535–6546 (1992).
19. R. R. Anderson, "Polarized-light examination and photography of skin," *Arch. Dermatol.* **127**, 1000–1005 (1991).
20. S. L. Jacques, L. H. Wang, D. V. Stephens, and M. Ostermeyer, "Polarized light transmission through skin using video reflectometry:

toward optical tomography of superficial tissue layers," in *Lasers in Surgery: Advanced Characterization, Therapeutics, and Systems VI*, R. R. Anderson, Ed., *Proc. SPIE* **2671**, 199–220 (1996).
21. S. G. Demos and R. R. Alfano, "Optical polarization imaging," *Appl. Opt.* **36**, 150–155 (1997).
22. S. L. Jacques, J. C. Ramella-Roman, and K. Lee, "Imaging skin pathology with polarized light," *J. Biomed. Opt.* **7**, 329–340 (2002).
23. A. H. Hielscher, J. R. Mourant, and I. J. Bigio, "Diffuse polarization spectroscopy on tissue phantoms and biological cell suspensions," in *Optical Biopsies and Microscopic Techniques*, I. J. Bigio, W. S. Grundfest, H. Schneckenburger, K. Svanger, and P. M. Viallet, Eds., *Proc. SPIE* **2926**, 67–76 (1996).
24. A. H. Hielscher, J. R. Mourant, and I. J. Bigio, "Influence of particle size and concentration on the diffuse backscattering of polarized light from tissue phantoms and biological cell suspensions," *Appl. Opt.* **36**, 125–135 (1997).
25. A. H. Hielscher, A. A. Eick, J. R. Mourant, J. P. Freyer, and I. J. Bigio, "Biomedical diagnostic with diffusely backscattered linearly and circularly polarized light," *Proc. SPIE* **2976**, 298–305 (1997).
26. M. G. Ducros, J. D. Marsack, H. G. Rylander III, S. L. Thomsen, and T. E. Milner, "Primate retina imaging with polarization-sensitive optical coherence tomography," *J. Opt. Soc. Am. A* **18**, 2945–2956 (2001).
27. P. A. Campochiaro, "Retinal and choroidal neovascularization," *J. Cell Physiol.* **184**, 301–310 (2002).
28. K. K. Glinworth, "The eye," in *Pathology*, 2nd ed., E. Rubin and J. L. Farber, Eds., pp. 1457–1502, J. B. Lippincott, Philadelphia (1994).
29. M. J. Rakovic, G. W. Kattawar, M. Mehbueoglu, B. D. Cameron, L. V. Wang, S. Rastegar, and G. L. Cote, "Light backscattering polarization patterns from turbid media: theory and experiment," *Appl. Opt.* **38**, 3399–3408 (1999).
30. D. S. Greenfield, R. W. Kington, and X.-R. Huang, "Effect of corneal polarization axis on assessment of retinal nerve fiber layer thickness by scanning laser polarimetry," *Am. J. Ophthalmol.* **129**, 715–722 (2000).
31. A. W. Dreher and K. Reiter, "Scanning laser polarimetry of retinal nerve fiber layer," *Proc. SPIE* **1746**, 34–41 (1992).
32. A. W. Dreher and K. Reiter, "Retinal laser ellipsometry: a new method for measuring the retinal nerve fiber layer thickness distribution," *Clin. Vision Sci.* **7**, 481–488 (1992).
33. D. K. Sardar, F. S. Salinas, J. J. Perez, and A. T. C. Tsin, "Optical characterization of bovine retinal tissues," *J. Biomed. Opt.* **9**, 624–631 (2004).
34. J. F. Beek, H. J. Staveren, P. Posthumus, H. J. C. M. Sternborg, and M. J. C. van Gemert, "In vitro double-integrating-sphere optical properties of tissue between 630 and 1064 nm," *Phys. Med. Biol.* **42**, 2255–2261 (1997).
35. S. A. Prahl, M. Keijzer, S. L. Jacques, and A. J. Welch, "A Monte Carlo model of light propagation in tissues," SPIE Institute Series **IS 5**, pp. 102–111 (1989).